Supplement of Biogeosciences, 22, 5921–5941, 2025 https://doi.org/10.5194/bg-22-5921-2025-supplement © Author(s) 2025. CC BY 4.0 License.





## Supplement of

## Distribution and sources of organic matter in submarine canyons incising the Gulf of Palermo, Sicily: A multi-parameter investigation

Sarah Paradis et al.

Correspondence to: Sarah Paradis (sparadis@ethz.ch)

The copyright of individual parts of the supplement might differ from the article licence.

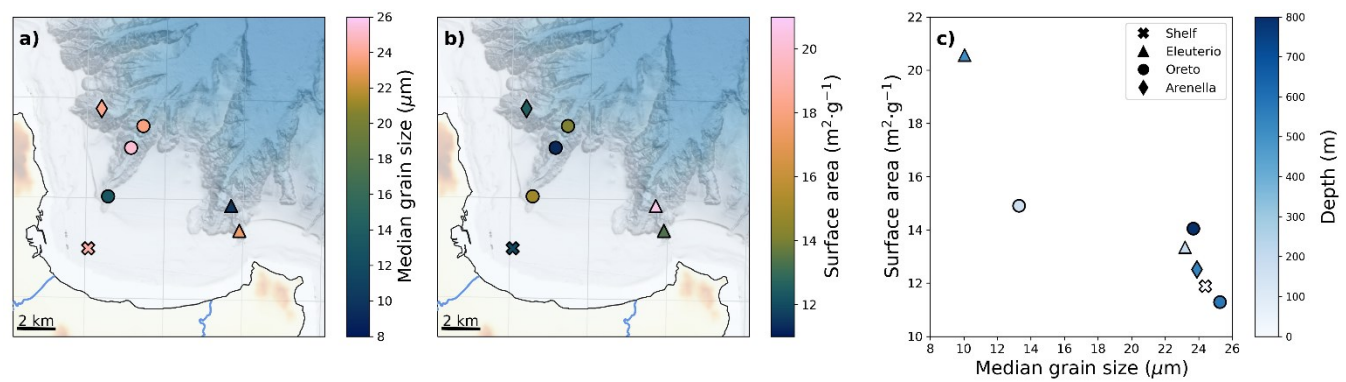
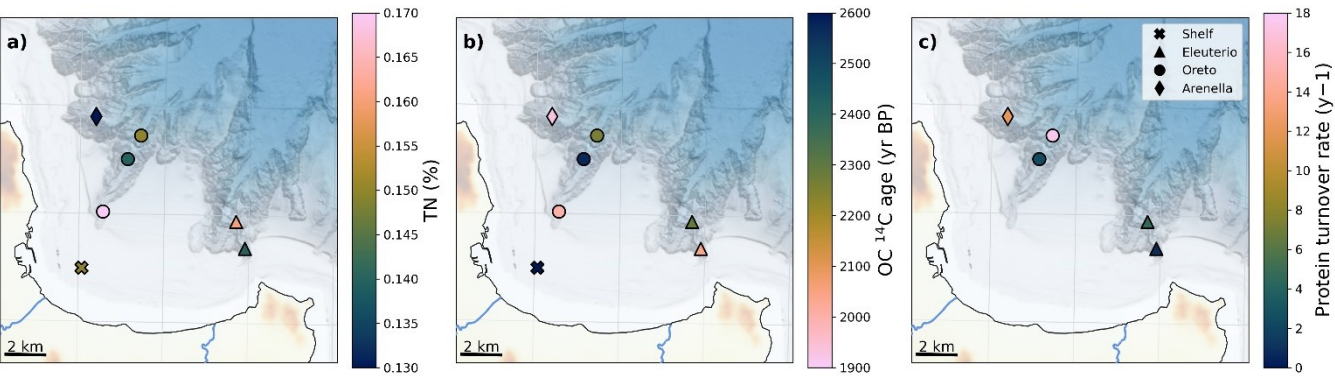


Figure S1. Spatial distribution of a) median grain size and b) mineral surface area. c) Relationship between median grain size and mineral surface area. Colour bars are adjusted to highlight the minimum, mean, and maximum values for each variable.



5 Figure S2. Spatial distribution of bulk parameters: a) TN, b) radiocarbon age, and c) protein turnover rate. Colour bars are adjusted to highlight the minimum, mean, and maximum values for each variable.

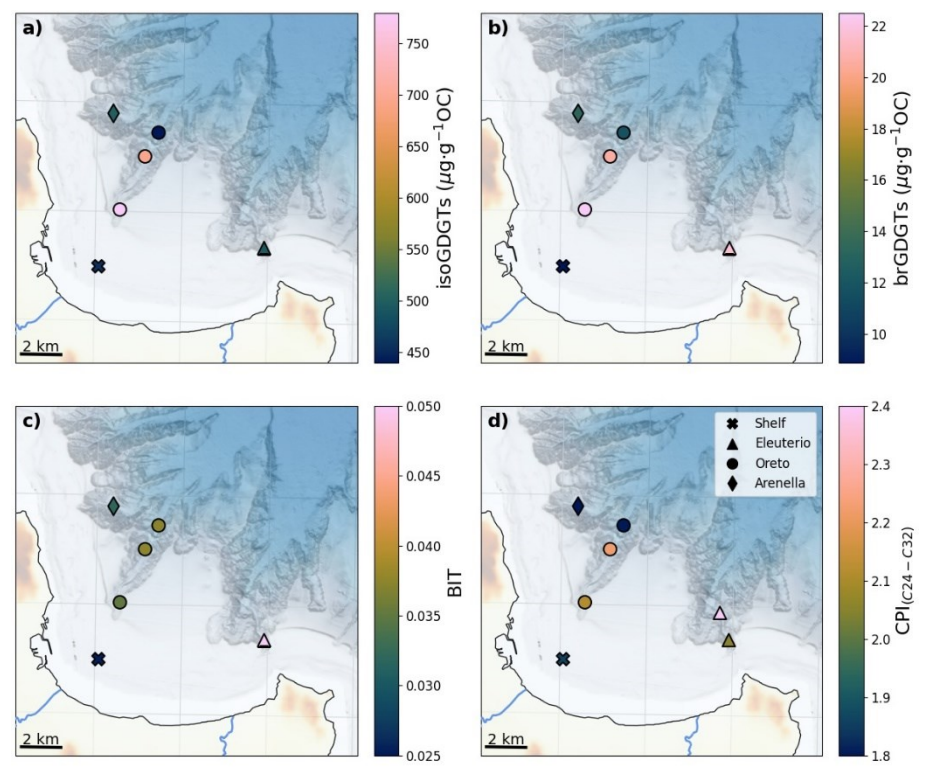


Figure S3. Spatial distribution of composition of GDGT and HMW FA proxies: a) isoGDGT concentrations, b) brGDGT concentrations, c) BIT index, and d) CPI<sub>(C24-C32)</sub> of HMW FA. Colour bars are adjusted to highlight the minimum, mean, and maximum values for each variable.

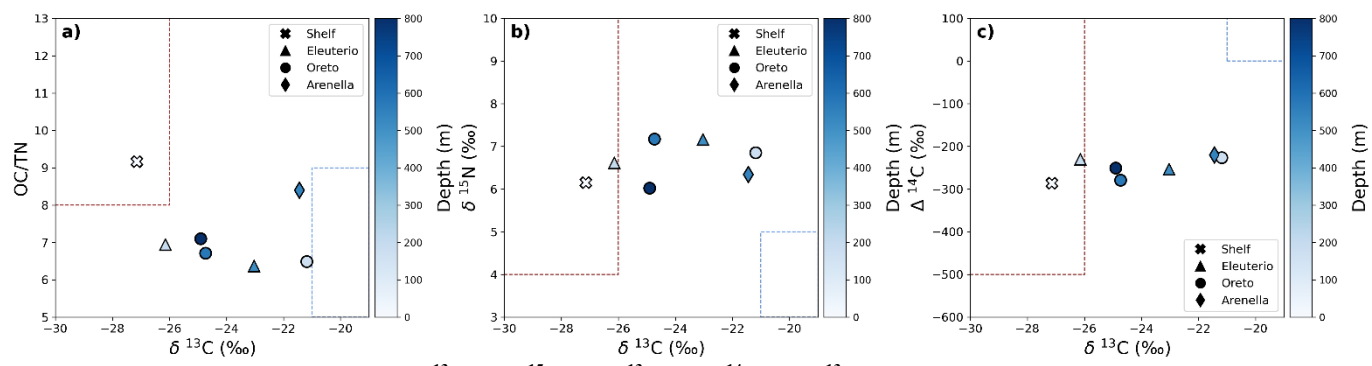


Figure S4. Scatter plots of OC/TN and  $\delta^{13}$ C (a),  $\delta^{15}$ N and  $\delta^{13}$ C (b),  $\Delta^{14}$ C and  $\delta^{13}$ C (d) used for the two-dimension mixing models, showcasing the values of terrestrial (brown dashed lines) and marine (blue dashed lines) endmembers. See Table 1 for the values and sources of the different endmember values.

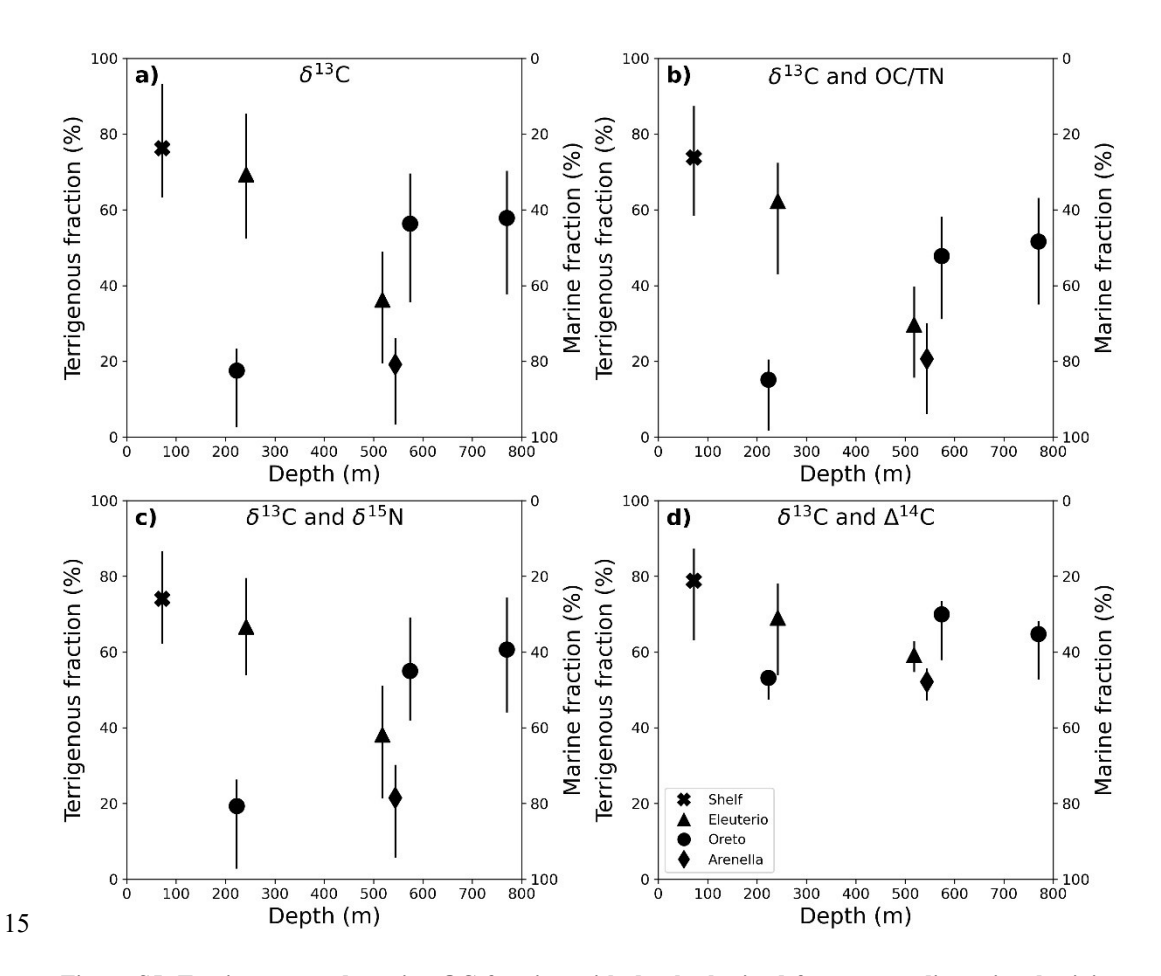


Figure S5. Terrigenous and marine OC fraction with depth obtained from a one-dimensional mixing model with  $\delta^{13}C$  (a), two-dimensional mixing model with  $\delta^{13}C$  and OC/TN (b),  $\delta^{13}C$  and  $\delta^{15}N$  (c),  $\delta^{13}C$  and  $\Delta^{14}C$  (d).

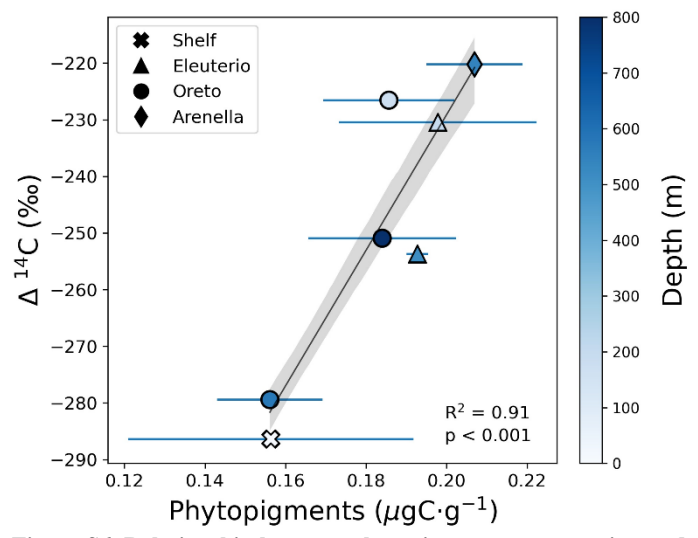


Figure S6. Relationship between phytopigment concentration and  $\Delta^{14}$ C, and fitting using a weighed-least squares regression, using the uncertainties from phytopigment concentrations as weights.

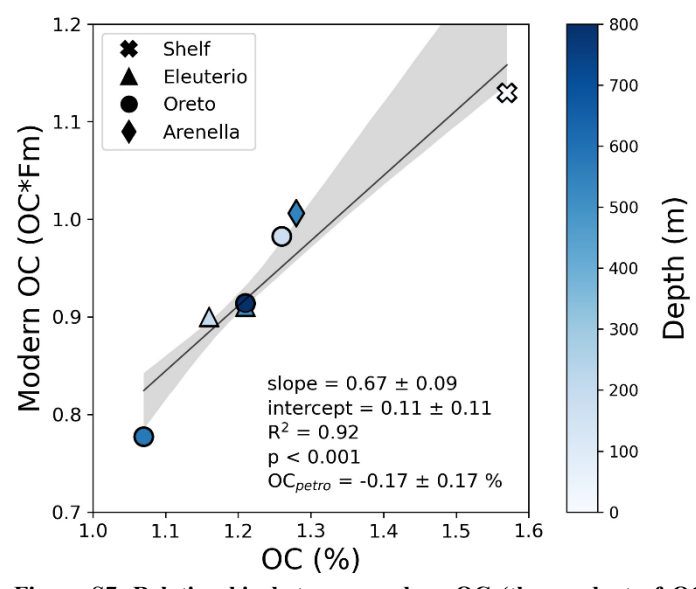


Figure S7. Relationship between modern OC (the product of OC content and radiocarbon fraction modern) and OC content. According to the fraction modern mixing model, the intercept of the fitting on the X-axis give the petrogenic OC content (Galy et al., 2008).

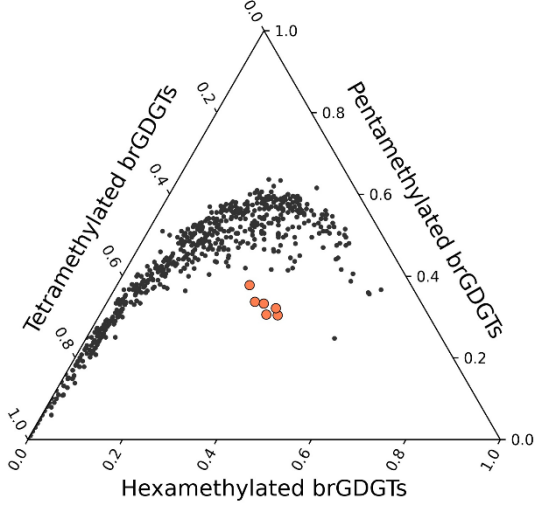


Figure S8. Ternary diagram showing the tetra-, penta-, and hexa-methylated brGDGTs in surface sediments of the Gulf of Palermo (pink circles) plotted together with the global soil and peat dataset (black dots) (Dearing Crampton-Flood et al., 2020). The clear offset of the Gulf of Palermo samples points to brGDGTs produced in-situ rather than being representative of soil-derived GDGTs.

Table S1. Sediment core sampling location, date, and subcore sampling strategy.

Core	Location	Coordinates		Depth (m)	Sampling date	Number of
		Latitude (N)	Longitude (E)	-		cores
S-70	Inner shelf	38.1248	13.4018	72	15/08/2016	1
AC-500	Mid-Arenella Canyon	38.1949	13.4090	544	16/08/2016	3
OC-200	Upper Oreto Canyon	38.1509	13.4140	223	15/08/2016	1
OC-500	Mid-Oreto Canyon	38.1754	13.4281	574	10/08/2016	3
OC-800	Lower Oreto Canyon	38.1864	13.4357	770	15/08/2016	1
EC-200	Upper Eleuterio Canyon	38.1347	13.4978	242	08/08/2016	1
EC-500	Mid-Eleuterio Canyon	38.1471	13.4924	518	08/08/2019	3

## References

30

Dearing Crampton-Flood, E., Tierney, J. E., Peterse, F., Kirkels, F. M. S. A. and Sinninghe Damsté, J. S.: BayMBT: A Bayesian calibration model for branched glycerol dialkyl glycerol tetraethers in soils and peats, Geochim. Cosmochim. Acta, 268, 142–159, doi:10.1016/j.gca.2019.09.043, 2020.

Galy, V., Beyssac, O., France-Lanord, C. and Eglinton, T.: Recycling of Graphite During Himalayan Erosion: A Geological Stabilization of Carbon in the Crust, Science (80-.)., 322(5903), 943–945, doi:10.1126/science.1161408, 2008.